eng

MDPI

Article

Kinetics of Heavy Rare Earth Element Extraction from Phosphoric Acid Solutions

Olga Cheremisina [1], Elena Lukyantseva [2,*] and Vasiliy Sergeev [1]

[1] The Department of General and Physical Chemistry, Empress Catherine II Saint Petersburg Mining University, 21st Line, 2, Saint Petersburg 199106, Russia; cheremisina_ov@pers.spmi.ru (O.C.); sergeev_vv2@pers.spmi.ru (V.S.)
[2] The Department of Chemical Technology and Energy Processing, Empress Catherine II Saint Petersburg Mining University, 21st Line, 2, Saint Petersburg 199106, Russia
* Correspondence: lukyantseva_lena@inbox.ru; Tel.: +7-(950)-512-64-99

Abstract

Rare earth elements are indispensable for a wide range of advanced technologies, which underscores their strategic importance. This study investigates the kinetics of extracting heavy rare earth elements—lutetium, thulium, yttrium, erbium, and dysprosium—from industrial phosphoric acid solutions generated during apatite processing. A comparative approach using both solvent and solid-phase extraction with di-(2-ethylhexyl)phosphoric acid (D2EHPA) was applied to elucidate the underlying mechanisms. Optimal solvent extraction parameters (V_{aq} : V_{org} = 2:1, φ_{D2EHPA} = 0.2, 298 K, stirring at 350 rpm) achieved efficiencies exceeding 85%. Efficient solid-phase recovery was attained under mild conditions (298 K, m:V = 1:10, shaking at 100 opm). The rate-limiting steps were identified as diffusion-controlled for solvent extraction, governed primarily by agitation intensity, and as a mixed external–internal diffusion regime for solid-phase extraction. Calculated activation energies for each element corroborate these findings.

Keywords: rare earth elements; phosphoric acid solution; solvent extraction; solid-phase extraction; kinetics; activation energy

1. Introduction

Rare earth elements (REEs), comprising the lanthanides, yttrium, and scandium, constitute a group of metals of exceptional technological and strategic importance. For decades, they have been indispensable for sustaining and advancing high-tech industries worldwide. Their unique physical and chemical properties are essential for diverse applications, including metallurgy, electrical engineering, petroleum refining, and green energy. Among these, the heavy rare earth elements (HREEs) are of particular significance due to their critical role in high-performance applications and their geopolitical supply risk [1]. For instance, dysprosium is a critical component in permanent magnets for wind turbines [2], yttrium enhances the hardness and wear resistance of structural ceramics [3], gadolinium improves the mechanical properties of specialty alloys [4], and ytterbium serves as a key dopant for laser crystals in solid-state and fiber laser applications [5].

Global demand for rare earth elements continues to rise steadily [6,7]. To meet this demand, production volumes have increased significantly, by approximately 89% between 2019 and 2023 [8] and reaching an estimated 390,000 tons in 2024 according to the U.S. Geological Survey [9]. This growing demand, coupled with the geographical concentration of mining and processing capabilities, notably in China, has led major economic blocs such

Check for updates

Academic Editor: Behzad Vaziri Hassas

Received: 23 December 2025
Revised: 17 January 2026
Accepted: 21 January 2026
Published: 27 January 2026

Copyright: © 2026 by the authors. Licensee MDPI, Basel, Switzerland. This article is an open access article distributed under the terms and conditions of the Creative Commons Attribution (CC BY) license.

as the European Union to classify REEs as critical raw materials, highlighting concerns over supply security [10].

To diversify supply beyond traditional ores, promising sources of rare earth elements are the process solutions generated during the acid leaching of apatite or other mineral concentrates [11–13]. Utilizing these solutions for REEs co-extraction offers a dual benefit: it yields an additional valuable product while enhancing the purity of the industrial streams for subsequent processing [14]. The primary methods for metal recovery from such aqueous feeds are solvent extraction [15,16] and sorption [17,18]. Given that these leachates typically feature low REE concentrations alongside a complex background of competing ions, solvent extraction using selective organic reagents remains one of the most widely applied recovery methods [19–21].

Phosphate ores represent a critical global resource and a major potential source of rare earth elements. Russia's extensive apatite deposits form a significant part of this resource base and could play a key role in mitigating the current REE supply deficit [22]. While Russia presently extracts REEs mainly from loparite ore [23], the largest portion of its total resources is contained in phosphate ores and remains largely unexploited. It is estimated that annual phosphoric acid production results in the loss of approximately 56,000 tons of REEs (including 23,000 tons of HREEs) to process streams.

The commercial viability of recovering REEs from such phosphate sources depends on both the economics of ore beneficiation and the efficiency of the downstream extraction process. While research to date has demonstrated the technical feasibility of co-extracting REEs as a by-product [24,25], modern industrial practices still result in significant losses. Typically, the heavy REE fraction predominantly remains in the phosphoric acid used for fertilizer production, whereas light REEs are largely discarded with the solid phosphogypsum waste [26]. Consequently, developing efficient technologies for the comprehensive utilization of these process solutions represents a critical step toward sustainable development, aligning with the principles of rational environmental management and the transition to zero-waste processes in metallurgy.

Industrial phosphoric acid solutions are notably enriched with heavy rare earth elements, whose supply–demand gap is particularly acute [27]. This makes such solutions a highly promising target for recovery research. For operations involving concentrated phosphoric acid media, di-(2-ethylhexyl)phosphoric acid (D2EHPA) has been established as the most effective extractant [28].

However, the pronounced physicochemical similarity of rare earth elements means that thermodynamic data alone are insufficient to ensure their efficient recovery and separation, as the process can be kinetically limited. Therefore, identifying the rate-limiting step, which governs the overall extraction kinetics, is critical for elucidating the underlying mechanism and enabling process optimization.

The rate-limiting step in a heterogeneous extraction process can be either diffusion, chemical reaction, or a combination of both. A diffusion-controlled regime is marked by strong dependence on stirring intensity and a low apparent activation energy E_a (usually below 20 kJ/mol). Conversely, a chemically controlled regime exhibits weak dependence on agitation and a higher E_a (typically above 40 kJ/mol). Intermediate values suggest mixed control, where both mass transfer and reaction kinetics are significant [29].

The mechanism and physicochemical principles of REE extraction have been thoroughly investigated various media [30,31]. For instance, in chloride media, the extraction of Nd(III) was found to be diffusion-controlled at the interface [32]. Similarly, a study in nitrate media using tributyl phosphate demonstrated that the process rate is determined by complex formation at the phase interface [33]. It is widely recognized that in

many solvent extraction systems, the key chemical interactions occur specifically at the interfacial region [34,35].

Furthermore, the role of kinetics remains critical beyond the extraction stage itself. For example, an investigation in nitric media showed that the stripping rate of neodymium is nearly two orders of magnitude faster than that of lanthanum, enabling their effective separation [36]. Kinetic considerations are also pivotal for separating elements with similar properties or isolating trace components from impurities. For example, one study demonstrated the separation of yttrium from iron (separation factor of 23) by exploiting their different rate-limiting steps at low temperature [37]. Another showed that increasing temperature accelerates the extraction of lanthanum more significantly than that of nickel, favoring their separation at higher temperatures [38].

However, such kinetic details are lacking for phosphoric acid media. The high ionic strength, strong complexing power of phosphate anions, low pH, and complex composition can fundamentally alter the extraction kinetics. Therefore, kinetic parameters from other systems are not directly applicable, necessitating a dedicated investigation in this industrially relevant yet poorly understood phosphoric acid medium.

In addition to the fundamental kinetic knowledge gap, practical considerations also motivate the exploration of alternative methods. A significant drawback of conventional solvent extraction is the reliance on toxic and volatile organic diluents, such as kerosene. This has spurred interest in alternative methods that eliminate the need for phase separation, including the use of ionic liquids [39] and, notably, solid-phase extractants, which avoid the use of liquid organic diluents entirely.

The aim of this work is to investigate the kinetics of heavy rare earth element extraction from industrially relevant phosphoric acid solutions derived from apatite processing. The study provides a comparative analysis of two recovery methods: conventional solvent extraction and solid-phase extraction, both utilizing di-(2-ethylhexyl)phosphoric acid as the active agent. The specific objectives are to identify the rate-limiting steps, calculate the apparent activation energies, and establish optimal conditions for the efficient extraction and potential separation of lutetium, thulium, yttrium, erbium, and dysprosium.

2. Materials and Methods

2.1. Preparation and Composition of Simulated Solutions

The extraction kinetics were studied using simulated industrial phosphoric acid solutions. Their composition was based on wet-process phosphoric acid derived from the sulfuric acid leaching of apatite concentrate, according to operational data provided by PJSC "PhosAgro" (The Balakovo Branch of Apatit, Saratov Region, Russia). The target composition is summarized in Table 1 and is characterized by a high concentration of phosphoric acid, a significant content of sulfuric acid, and a complex mixture of minor impurities (F, Al, Ca, Fe, Si). The total rare earth oxide (TREO) content ranges from 0.07 to 0.10%.

The relative distribution of individual rare earth elements within this total, also provided by the industrial partner, is given in Table 2. This distribution is dominated by light REEs, whereas the target heavy REEs of this study (Y, Dy, Er, Tm, Lu) collectively account for approximately 16% of the TREO.

Given the primary objective of this work—a fundamental kinetic analysis of individual heavy rare earth elements—a simplified model solution was rationally employed. The model faithfully replicates the aggressive and constant chemical background of the industrial stream: 4.5 M H_3PO_4 and 0.19 M H_2SO_4. This preserves the most critical and challenging aspect of the real system, namely the highly acidic, high-ionic-strength phosphate matrix. However, to eliminate cross-interference and allow precise determination of kinetic parameters for each element, the complex multi-component mixture of REEs present

in the industrial feed was substituted with single-element solutions of the target HREEs: lutetium, thulium, yttrium, erbium, and dysprosium. The REE concentrations in these solutions ranged from 2 to 5 mmol/L, reflecting their typical content in the industrial feed.

Table 1. Composition of the industrial phosphoric acid stream.

Component	Content, %
P_2O_5	26–28
SO_3	1.2–1.8
F	1.4–1.5
Al_2O_3	0.1–0.4
CaO	0.3–0.8
Fe_2O_3	0.3–0.4
SiO_2	0.8–1.1
TREO	0.07–0.10

Table 2. Relative distribution of REEs in the total rare earth oxides.

Oxide	Content, rel.%	Oxide	Content, rel.%
La_2O_3	15.07	Dy_2O_3	1.92
Ce_2O_3	37.24	Ho_2O_3	0.34
Pr_2O_3	4.67	Er_2O_3	0.88
Nd_2O_3	18.31	Y_2O_3	12.51
Sm_2O_3	3.08	Yb_2O_3	0.51
Eu_2O_3	0.96	Tm_2O_3	0.32
Gd_2O_3	3.37	Lu_2O_3	0.39
Tb_2O_3	0.43		

Accordingly, the model solutions were prepared by dissolving a calculated mass of high-purity rare earth nitrate salt ($Ln(NO_3)_3 \cdot xH_2O$, 99.9%, JSC LenReactiv, Saint Petersburg, Russia) in distilled water to prepare individual REE stock solutions. The exact concentration of each of them was verified by direct complexometric titration with ethylenediaminetetraacetic acid (EDTA). A standard EDTA titrant solution (0.05 M) was prepared from a fixanal. For the titration, a 5 mL aliquot was mixed with 3 mL of a 0.1% ascorbic acid solution to reduce potential interfering ions, followed by the addition of 20 mL of an ammonium acetate-acetic acid buffer (pH 5.5). Xylenol orange (0.1% aqueous solution, alkalized) was used as a metallochromic indicator, and 5–7 drops were added to the mixture, imparting a violet color. The solution was then titrated with EDTA under constant stirring until the color changed sharply from violet to clear yellow, marking the endpoint. Each titration was performed in duplicate, and the average value was used to calculate the precise metal concentration.

2.2. Extraction Experiments and Kinetic Studies

The organic phase for solvent extraction consisted of di-(2-ethylhexyl)phosphoric acid (purity $\geq$ 95%, Leap Chem Co., Ltd., Hangzhou, China) dissolved in a commercial kerosene diluent (TS-1 grade). Prior to each experiment, the extraction mixture was prepared ex situ in a separate vessel by combining the extractant and diluent at a predetermined volume ratio.

Extraction experiments were performed using an automated Parallel Auto-MATE Reactor System (H.E.L Group, Hemel Hempstead, UK). A schematic of the setup is presented in Figure 1. The system comprises a reactor equipped with a magnetic stirrer, an electric heater, and a thermocouple for precise temperature control, and is designed to handle reaction mixtures with volumes up to 200 mL. An extraction experiment involved contacting the simulated aqueous solution with the organic phase in the reactor, with aqueous samples periodically withdrawn for kinetic analysis.

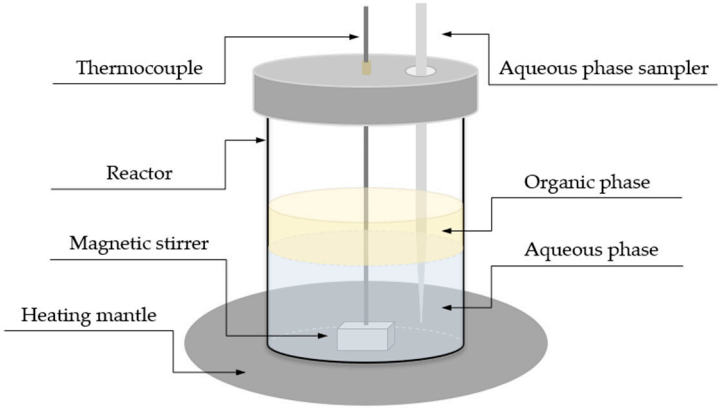


Figure 1. Experimental setup for solvent extraction.

For solid-phase extraction, a ready-to-use polymeric sorbent impregnated with D2EHPA (Seplite LXCL-204, Sunresin New Materials Co., Ltd., Xi'an, China) was used. This material, provided directly by the production facility, is supplied as opaque white spherical beads with a bulk density of 0.4 g/mL.

A precisely weighed amount of the sorbent was measured using an analytical balance with a readability of ± 0.0001 g and then mixed with the simulated solution in an Erlenmeyer flask together with a measured volume of the simulated aqueous solution. The flasks were then secured in a thermostated Shaking Incubator 3032 (GFL, Grossburgwedel, Germany), which provided orbital shaking to ensure consistent contact between the solid and aqueous phases (Figure 2). Upon completion of the extraction period, the sorbent was separated by filtration, and the resulting aqueous phase was analyzed.

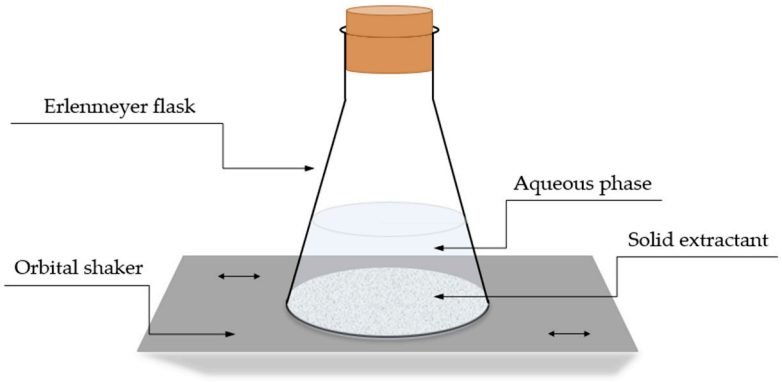


Figure 2. Experimental setup for solid-phase extraction in a temperature-controlled incubator.

The concentration of rare earth elements in the phosphoric acid solutions, both before and after extraction, was determined by X-ray fluorescence spectrometry using a PANalytical Epsilon 3 energy-dispersive spectrometer (Malvern Panalytical Ltd., Almelo, The Netherlands). This technique allows for the analysis of elements from Na to Am in concentrations ranging from 10^{-4} to 100 wt.%.

To account for matrix effects such as absorption and spectral interference, a multi-point calibration was performed for each REE. Primary stock solutions were prepared from high-purity salts, and their concentrations were verified by complexometric titration with EDTA. Working standards were prepared by into a matrix-matched solution of 4.5 M H_3PO_4 and 0.19 M H_2SO_4, covering a concentration range from 0 to 0.5 M for each element.

The limits of detection and quantification were determined as three and ten times the standard deviation of the background signal, respectively, and were found to be <0.5 mmol/L for all REEs. Accuracy and precision were confirmed using independently prepared check standards and replicate measurements, yielding a relative standard deviation typically below 3%. Final quantification was performed by the instrument's software using the fundamental parameters method with matrix corrections.

The extraction efficiency (E, %) for each element was calculated according to the following formula:

$$E = \left(1 - \frac{C_{aq}}{C_0}\right) \cdot 100\%, \quad (1)$$

where C_0 and C_{aq} are initial and final concentrations of metals in the aqueous phase.

The apparent activation energy E_a was calculated from rate constants determined at two temperatures using a two-point form of the Arrhenius equation. The derivation begins with the standard form for each temperature:

$$k = \mathrm{A} \cdot e^{\left(-\frac{E_a}{RT}\right)}. \quad (2)$$

Taking the natural logarithm of the ratio k_2/k_1 and simplifying yields:

$$\ln\left(\frac{k_2}{k_1}\right) = \frac{E_a}{R} \cdot \left(\frac{1}{T_1} - \frac{1}{T_2}\right). \quad (3)$$

Solving for E_a yields the expression used in this study:

$$E_a = \ln\left(\frac{k_2}{k_1}\right) \frac{RT_1T_2}{T_2 - T_1}, \quad (4)$$

where R is the universal gas constant, J/(mol·K), T_1 and T_2 are the extraction temperatures (K), k_1 and k_2 are the reaction rate constants.

3. Results

3.1. Solvent Extraction

3.1.1. Optimization of Extraction Parameters

The extraction efficiency in solvent extraction is predominantly governed by two key parameters: the extractant concentration in the organic phase and the aqueous-to-organic phase ratio ($V_{aq} : V_{org}$). To determine the optimal conditions for the kinetic study, preliminary equilibrium experiments were conducted at 298 K, a stirring speed (w) of 350 rpm, and a contact time of 20 min.

Initial tests were performed using aqueous solutions of lutetium and erbium contacted with an organic phase containing D2EHPA at varying volume fractions (φ), while maintaining a constant phase ratio of $V_{aq} : V_{org}$ of 2:1. The results are presented in Figure 3.

Lutetium extraction exceeded 85% efficiency at a relatively low extractant concentration (φ = 0.2). In contrast, achieving a comparable efficiency for erbium required a significantly higher D2EHPA fraction ($\varphi \geq 0.6$). This pronounced difference indicates that using a moderately concentrated organic phase (e.g., 20 vol% D2EHPA) could enable the selective recovery of heavier REEs (starting with Lu), forming a basis for their potential sequential separation.

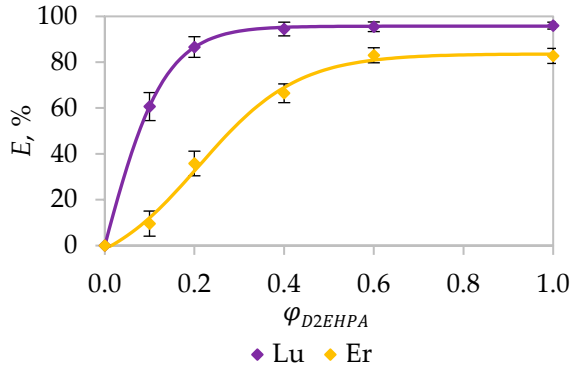


Figure 3. Extraction efficiency (E, %) of Er and Lu as a function of the volume fraction (φ) of D2EHPA in the kerosene diluent. Experimental conditions: $C_{H_3PO_4}$ = 4.5 M, V_{aq} : V_{org} = 2:1, w = 350 rpm, T = 298 K.

Subsequently, the influence of the phase ratio was evaluated for erbium extraction (Figure 4). Although the maximum single-stage efficiency for erbium (~48%) was attained at a 1:1 phase ratio, the 2:1 ratio was selected for all further experiments. This choice offers a superior volumetric efficiency, allowing twice the volume of aqueous feed to be processed per unit volume of extractant while still achieving a substantial extraction yield (~36%), which is suitable for designing an efficient multi-stage counter-current process.

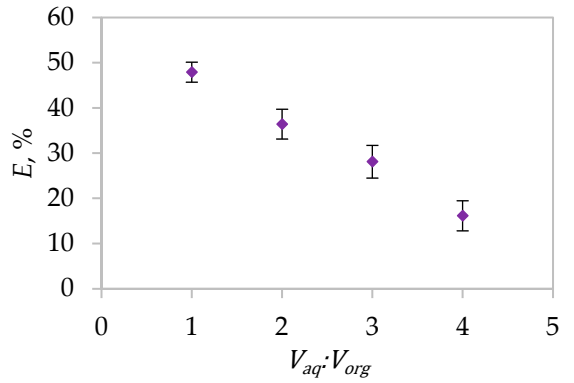


Figure 4. Extraction efficiency of Er as a function of the aqueous-to-organic phase volume ratio V_{aq}:V_{org}. Experimental conditions: $C_{H_3PO_4}$ = 4.5 M, φ_{D2EHPA} = 0.2, w = 350 rpm, T = 298 K.

3.1.2. Identification of the Rate-Limiting Steps

In kinetic studies of solvent extraction, the process is analyzed by plotting the approach to equilibrium (I) as a function of time (t), i.e., $I = f(t)$ [40]. The parameter I is calculated as follows:

$$I = \frac{C_{org}}{C^*_{org}} = \frac{(C_0 - C_{aq})}{\left(C_0 - C^*_{aq}\right)}, \quad (5)$$

where C^*_{org} and C^*_{aq} are the equilibrium concentrations in the organic and aqueous phases, respectively, and C_0 is its initial concentration in the aqueous solution.

The apparent rate constant k, which represents the extraction rate under constant mass transfer coefficients and interfacial area, was determined from the linearized form of the kinetic equation:

$$\ln(1 - I) = -\mathrm{k}t, \quad (6)$$

To identify the rate-limiting step in the extraction of rare earth elements, the extraction behavior of a series of heavy rare earth metals—lutetium, thulium, yttrium, erbium, and dysprosium—was investigated, with a focus on the effects of stirring intensity and temperature. All experiments were performed in at least duplicate, and the reported data

points represent the mean values. The standard deviation for replicate measurements did not exceed 4%.

The results (Figure 5) show that the extraction rate depends strongly on agitation up to an optimal range of 350–450 rpm, where equilibrium is attained within 3–5 min. This dependence is characteristic of a diffusion-controlled regime, where the rate is limited by mass transfer through the aqueous boundary layer. At lower stirring speeds (<350 rpm), equilibrium required at least 10 min. Speeds exceeding 450 rpm (e.g., 600 rpm) offered negligible kinetic improvement but induced emulsification, complicating phase separation.

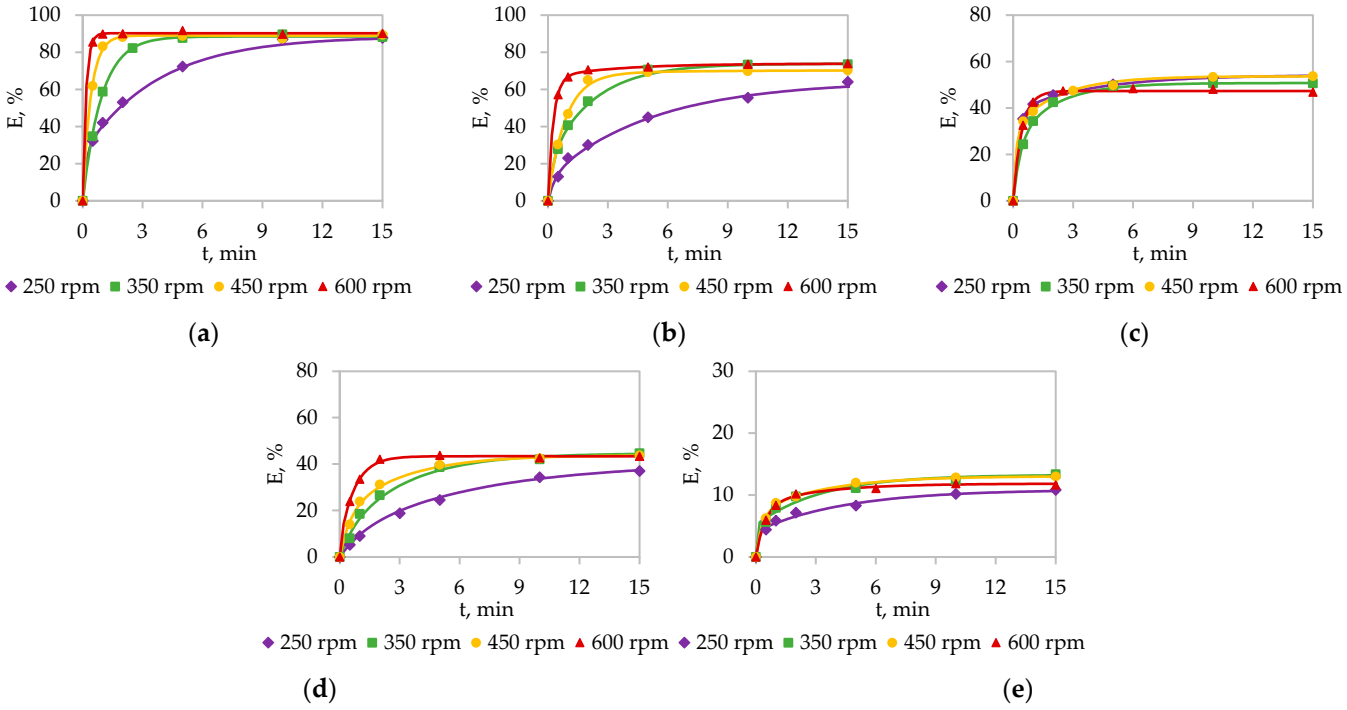


Figure 5. Extraction efficiency as a function of time at different stirring rates for (**a**) Lu; (**b**) Tm; (**c**) Y; (**d**) Er; (**e**) Dy. Experimental conditions: $C_{H_3PO_4}$ = 4.5 M, C_0 = 2–5 mmol/L, V_{aq} : V_{org} = 2:1, T = 298 K.

The investigation of temperature effects (Figure 6) within the range of 298 to 333 K demonstrated a trade-off. While elevated temperature moderately accelerated the extraction kinetics, it significantly reduced the thermodynamic equilibrium efficiency. This decrease is indicative of an exothermic extraction process. The complexation of rare earth cations (Ln^{3+}) with acidic organophosphorus extractants such as D2EHPA is generally exothermic. Consequently, according to Le Chatelier's principle, increasing the temperature shifts the equilibrium toward the endothermic reverse reaction (stripping), thereby lowering the apparent extraction constant and the final yield.

Across all variations in stirring intensity and temperature: the extraction efficiency decreased from approximately 90% for lutetium to 12% for dysprosium. This order follows the decreasing atomic number (and ionic radius) of the elements, a direct consequence of the lanthanide contraction. This strong inherent selectivity implies that the use of a moderately concentrated extractant could form the basis for a sequential separation strategy, enabling the preferential recovery of the heaviest rare earth elements first.

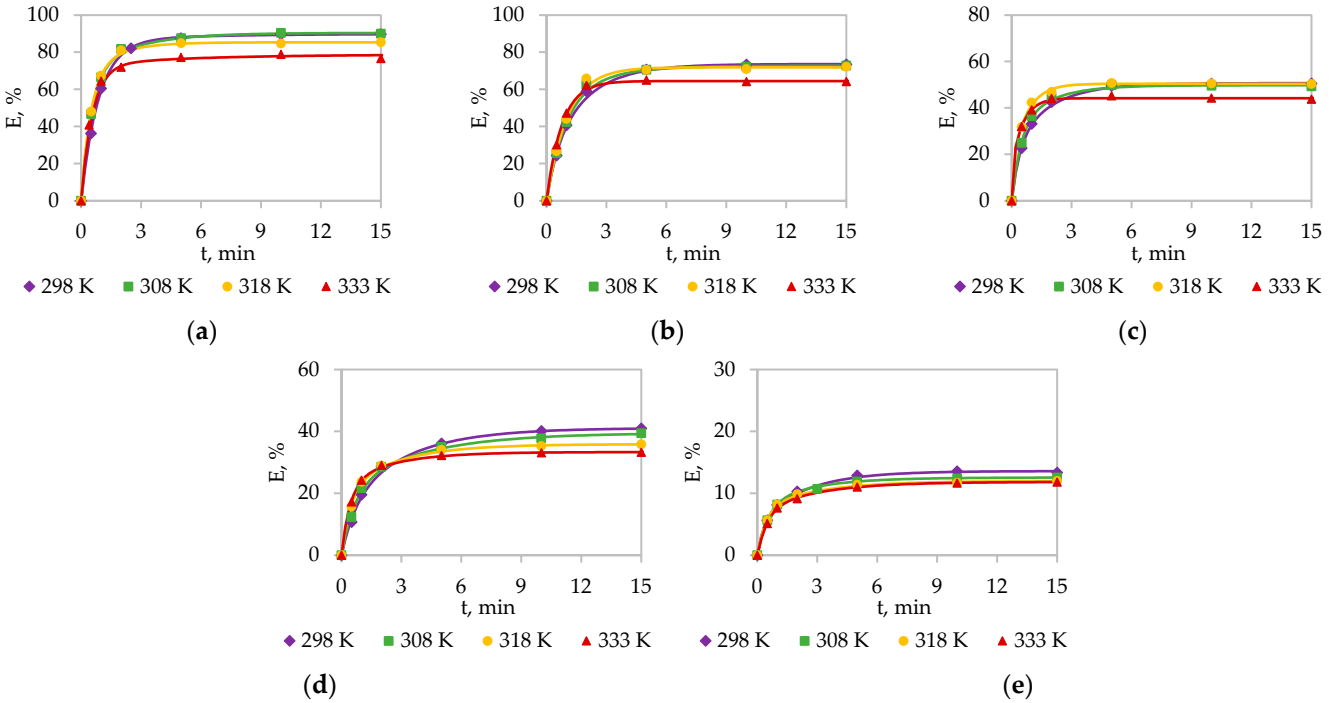


Figure 6. Extraction efficiency as a function of time at different temperatures for (**a**) Lu; (**b**) Tm; (**c**) Y; (**d**) Er; (**e**) Dy. Experimental conditions: $C_{H_3PO_4}$ = 4.5 M, C_0 = 2–5 mmol/L, V_{aq} : V_{org} = 2:1, w = 350 rpm.

3.2. Solid-Phase Extraction

3.2.1. Kinetic Modeling Strategy

The mechanism of rare earth element extraction using a solid-phase extractant comprises three sequential, potentially rate-limiting steps:

1. External diffusion across the aqueous boundary layer surrounding the extractant.
2. Internal diffusion through the pores of the polymeric matrix.
3. Chemical reaction with immobilized functional groups of D2EHPA.

To discriminate between these potential rate-limiting steps, the experimental kinetic data were fitted to a series of conventional models spanning both kinetic and diffusion-based types. The selection of models was based on their ability to describe specific mechanistic scenarios common in liquid-solid systems.

Pseudo-first-order and pseudo-second-order models were applied as standard empirical approaches to quantify overall sorption rates and capacities [41,42].

The pseudo-first-order model, based on the sorption capacity of the solid-phase extractant, is given by the following equation:

$$\ln(q_e - q_t) = \ln(q_e) - k_1 t, \quad (7)$$

where q_t and q_e are the sorption capacities (mg/g) at time t and at equilibrium, respectively, and k_1 is the pseudo-first-order rate constant (min^{-1}).

The pseudo-second-order model assumes that the extraction process follows pseudo-chemical reaction kinetics and is defined by the following equation:

$$q_t = \frac{q_e^2 k_2 t}{1 + k_2 q_{eq} t}, \quad (8)$$

where k_2 is the pseudo-second-order rate constant (g/(mg·min)). A higher value of k_2 indicates a shorter time required to reach equilibrium.

The Elovich model is applied to describe heterogeneous chemisorption kinetics typical for surfaces with a distribution of active site energies [43]. The model rests on two key premises: the energetic heterogeneity of the adsorbent surface and the negligibility of desorption and inter-ion interactions at low surface coverages:

$$q_t = \frac{1}{\beta} ln(\alpha\beta) + \frac{1}{\beta} ln(t), \quad (9)$$

where α is the initial sorption rate (mg/(g·min)) and β is the desorption constant (g/mg).

The Homogeneous Particle Diffusion Model accounts for both internal and external diffusion limitations [44].

The rate-limiting step of the extraction process can be identified by examining how the extraction conditions affect the value of the rate constant k, which is determined under constant mass transfer coefficients and a fixed interfacial area. For internal diffusion, the model takes the form $\ln(1 - I) = -kt$, whereas for external diffusion, it is described by $\ln(1 - q^2) = -kt$.

To gain deeper insight into the mechanism of solid-phase extraction and identify and quantify the contribution of diffusion within the polymer matrix, the intraparticle diffusion model by Weber-Morris is commonly applied [45]:

$$q_t = k_i \cdot t^{0.5} + C, \quad (10)$$

where k_i is the intraparticle diffusion rate constant (mg/(g·min$^{0.5}$)) and C is a constant related to the boundary layer resistance to mass transfer (mg/g).

For polymers with low porosity, which are effectively impermeable to the liquid-phase reagent, the extraction kinetics can be modeled using the shrinking core approach, also referred to as the progressive shell or shrinking particle model (SPM) [46,47]. As well as the Homogeneous Particle Diffusion model, it is tested to distinguish between a diffusion-limited process within a gel-like particle and a reaction-limited process at a receding interface.

SPM expresses the relationship between the reaction time and the fractional conversion through three different equations, each corresponding to a specific rate-limiting step.

1. Film diffusion:

$$t = \frac{br_0 C_{so}}{3 C_{A0} K_{mA}} X, \quad (11)$$

2. Diffusion through the product layer:

$$t = \frac{br_0^2 C_{so}}{6 D_{e,r} C_{A0}} \left[3 - 3(1 - X)^{2/3} - 2X\right], \quad (12)$$

3. Chemical reaction:

$$t = \frac{r_0}{k_s C_{A0}} \left[1 - (1 - X)^{1/3}\right], \quad (13)$$

where b is the stoichiometric coefficient of the reaction between metal ions in the solution and the extractant in the resin, C_{A0} is the initial concentration of metal ions (mol/L of solution), and C_{so} is the concentration of the extractant in the matrix (mol/g of resin).

This multi-model approach allows for a more robust diagnosis of the controlling mechanism than reliance on a single model.

3.2.2. Identification of the Rate-Limiting Steps

To determine the rate-limiting step in the solid-phase extraction and estimate the apparent activation energy, the extraction kinetics of lutetium, thulium, yttrium, erbium, and dysprosium were investigated, focusing on the influence of temperature. The experiments were performed using an orbital shaker at 100 oscillations per minute (opm). A solid-to-liquid ratio (m:V) of 1:10 was selected based on preliminary screening and prior experience with similar industrial phosphoric acid systems [37]. This ratio ensures sufficient sorbent capacity for reliable kinetic analysis while maintaining practical relevance for potential scale-up. Reported data points represent the mean values with a standard deviation not exceeding 4.5%.

The extraction efficiency as a function of time at different temperatures is shown in Figure 7.

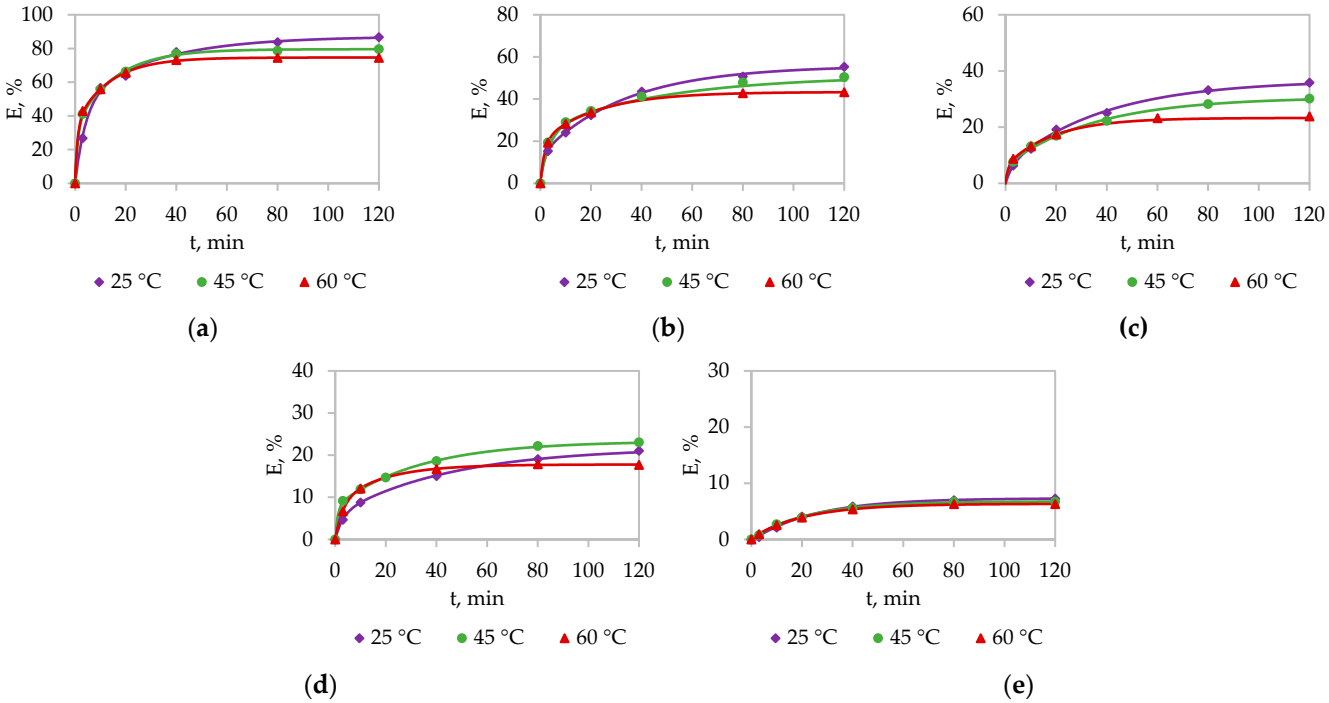


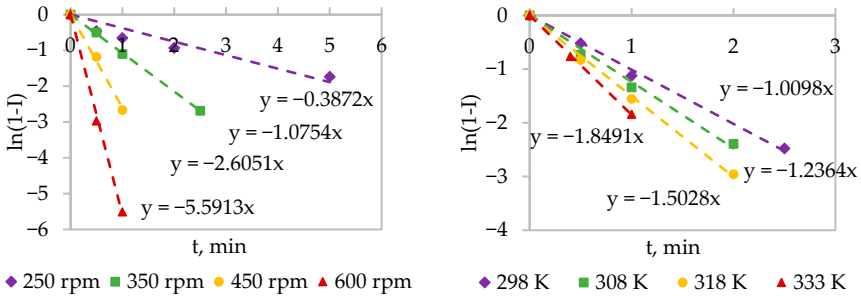
Figure 7. Extraction efficiency as a function of time at different temperatures for (**a**) Lu; (**b**) Tm; (**c**) Y; (**d**) Er; (**e**) Dy. Experimental conditions: $C_{H_3PO_4}$ = 4.5 M, m:V = 1:10, C_0 = 2–5 mmol/L, n = 100 opm.

4. Discussion

4.1. Kinetic Analysis and Mechanism of Solvent Extraction

To determine the rate-limiting step, the kinetic data were analyzed using the linearized form of the kinetic equation $\ln(1 - I) = -kt$. The initial linear region was used to determine the rate under conditions of a constant rate-limiting step and negligible back-reaction influence. This methodology ensures a consistent basis for comparative kinetic analysis of different elements and conditions. Representative kinetic plots for lutetium extraction are shown in Figure 8.

The slope of these linear plots, representing the apparent rate constant k, exhibited a significantly greater dependence on stirring intensity than on temperature. This observation strongly suggests that the overall extraction rate is limited by diffusion through the aqueous boundary layer. An identical dependence was confirmed for all other investigated heavy rare earth elements.



(**a**) (**b**)

Figure 8. Kinetic analysis of lutetium extraction: (**a**) Natural logarithm of the approach to equilibrium versus time at different stirring rates; (**b**) $\ln(1 - I)$ versus time at different temperatures. Experimental conditions: $C_{H_3PO_4}$ = 4.5 M, C_0 = 3.2 mmol/L, V_{aq}:V_{org} = 2:1, w = 350 rpm.

The activation energy for the extraction of each element was determined from an Arrhenius-type plot of ln$k$ versus the reciprocal of absolute temperature ($1/T$), as shown in Figure 9. The calculated activation energy values, summarized in Table 3, provide additional quantitative evidence for a diffusion-controlled rate-determining step.

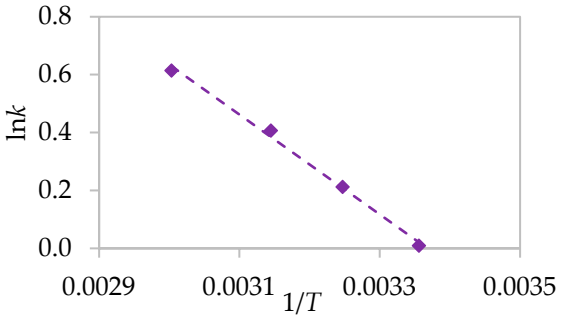


Figure 9. Arrhenius plot for lutetium extraction: natural logarithm of the apparent rate constant ln$k$ versus the reciprocal of absolute temperature ($1/T$, K^{-1}).

Table 3. Activation energies for the solvent extraction of HREEs from phosphoric acid solutions.

REE	E_a, kJ/mol
Lu	14.5 ± 0.4
Tm	10.5 ± 0.3
Y	23.1 ± 0.7
Er	18.2 ± 0.5
Dy	7.8 ± 0.2

4.2. Kinetic Analysis and Mechanism of Solid-Phase Extraction

The kinetic parameters derived from fitting the data to models (5–11), along with the coefficients of determination (R^2), are summarized in Table 4.

While pseudo-second-order kinetics are frequently used to model the solid-phase extraction of REEs from acidic media [42,48], the analysis performed in this work suggests a different rate-determining mechanism. The application of diffusion-based models—specifically, the homogeneous particle diffusion and Elovich models—yielded consistently high correlation coefficients (R^2). Moreover, the close correspondence between the experimental and model-predicted sorption capacities validates the use of these diffusion models. Collectively, these results strongly indicate that the extraction of heavy REE ions in this system is predominantly controlled by diffusion.

Table 4. Kinetic parameters for lutetium extraction using different models.

***T*, K**	**298**	**318**	**333**
Pseudo-first-order model (film diffusion)			
k, min^{-1}	0.047	0.060	0.119
R^2	0.854	0.902	0.962
Homogeneous particle diffusion model (internal/gel diffusion)			
k, min^{-1}	0.036	0.048	0.096
R^2	0.987	0.993	0.998
Pseudo-second-order model (chemical reaction)			
k, g/(mg·min)	0.017	0.050	0.125
R^2	0.932	0.842	0.797
Elovich model (heterogeneous particle diffusion)			
α, mg/(g·min)	22.379	29.375	39.618
β, g/mg	0.356	0.391	0.420
R^2	0.987	0.988	0.990
Shrinking core model (internal/gel diffusion control)			
k, min^{-1}	0.011	0.013	0.024
R^2	0.953	0.937	0.968
Shrinking core model (chemical reaction control)			
k, min^{-1}	0.010	0.012	0.022
R^2	0.875	0.873	0.918

A direct comparison of the two shrinking core model variants reveals that the internal (gel) diffusion-controlled mechanism provides a markedly superior fit to the experimental data over the chemical reaction-controlled mechanism. This result serves as an independent and compelling line of evidence reinforcing the conclusion of diffusion-limited kinetics.

The increase in the apparent rate constants for diffusion-based models with temperature indicates a reduction in diffusional resistance, a trend that is also influenced by the thermally activated nature of the chemical interaction at the functional sites. When modeling REE extraction kinetics with the Elovich equation, the parameter α is considered an alternative form of the "rate constant" [49]. The calculated values of α (initial sorption rate) also increase with rising temperature from 298 to 333 K, which suggests chemisorption behavior. Conversely, the reciprocal of the desorption constant ($1/\beta$), representing the number of available interaction sites, showed only a minor decrease.

The data in Table 4 show that the initial sorption rate significantly exceeds the corresponding desorption rate. This pronounced difference can be reasonably explained by the high initial availability and favorable accessibility of functional groups of D2EHPA on the surface of the polymeric matrix to lanthanide ions in the bulk solution.

To elucidate the extraction mechanism, the kinetics were analyzed using the Weber-Morris intraparticle diffusion model (Figure 10).

Linear regions of the corresponding plots do not extend over the full duration of the extraction process, demonstrating that intraparticle diffusion alone does not govern the overall kinetics. The observed deviations from linearity at the origin, along with the distinct multilinear segments, are characteristic of a process where both external (film) and internal (intraparticle) diffusion contribute significantly to the rate limitation [50]. The sorption dynamics are characterized by an initially fast uptake, followed by a pronounced deceleration. This trend is consistent with the progressive saturation of easily accessible

surface sites and the increasing diffusional resistance as pores within the polymer matrix become occupied.

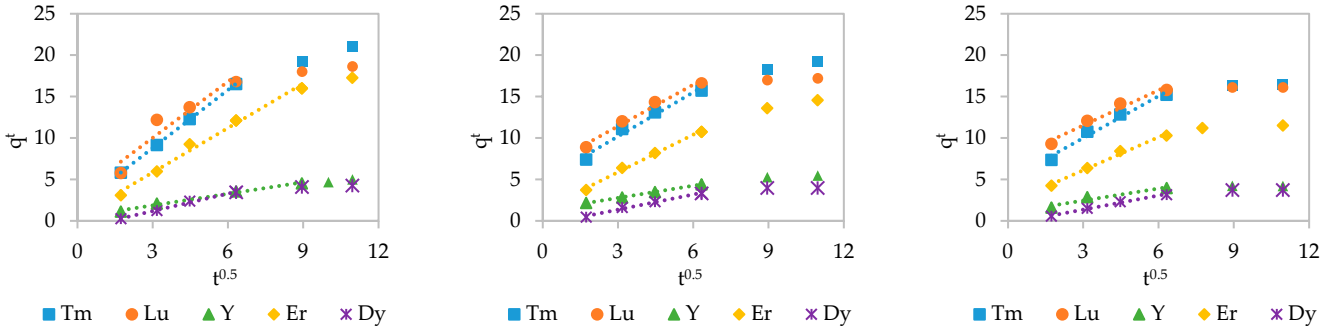


Figure 10. Kinetic analysis using the intraparticle diffusion model: sorption capacity q^t versus square root of time $t^{0.5}$ at (a) 298 K; (b) 318 K; (c) 333 K. Experimental conditions: $C_{H_3PO_4}$ = 4.5 M, m:V = 1:10, C_0 = 2–5 mmol/L, n = 100 opm.

A process is typically considered to be film-diffusion controlled when the activation energy is below 20 kJ/mol, while E_a values in the range of 20–40 kJ/mol suggest a mixed regime where diffusion plays a partial but significant role [44]. The activation energy values derived in this study from the Elovich and homogeneous particle diffusion models (see Table 5 and Figure 11) fall predominantly within the latter range. This result strongly supports the conclusion that the extraction kinetics are governed by a mixed mechanism involving both internal (intraparticle) and external (film) diffusion [48].

Table 5. Activation energies (E_a) for the solid-phase extraction of rare earth elements.

REE	*T*, K	E_a, kJ/mol
Lu	298–318	11.4 ± 0.2
	318–333	40.7 ± 0.7
Tm	298–318	8.0 ± 0.2
	318–333	31.2 ± 0.6
Er	298–318	2.3 ± 0.1
	318–333	33.6 ± 0.7
Y	298–318	16.2 ± 0.3
	318–333	33.3 ± 0.7
Dy	298–318	4.8 ± 0.2
	318–333	3.8 ± 0.1

The analysis of activation energies reveals a temperature-dependent shift in the extraction mechanism. At lower temperatures (298–318 K), the calculated E_a values (<20 kJ/mol) indicate a process predominantly limited by both intraparticle and film diffusion. However, as the temperature increases, the derive E_a rise, suggesting a transition to a mixed control regime, where the activation energy for the chemical reaction step becomes kinetically competitive with that of diffusion.

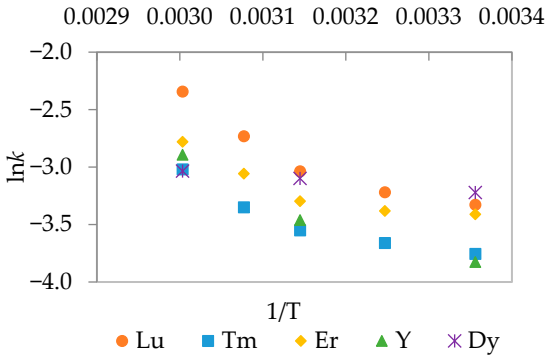


Figure 11. Arrhenius plot for solid-phase extraction: natural logarithm of the apparent rate constant ln$k$ versus the reciprocal of absolute temperature ($1/T$, K^{-1}). Experimental conditions: $C_{H_3PO_4}$ = 4.5 M, m:V = 1:10, C_0 = 2–5 mmol/L, n = 100 opm.

This transition can be attributed to the concurrent effects of temperature on the thermodynamics of the extraction reaction and the physical properties of the polymeric sorbent. First, the extraction with D2EHPA is exothermic; therefore, according to Le Chatelier's principle, increasing the temperature shifts the equilibrium toward the endothermic reverse reaction (stripping), effectively raising the energy barrier for the forward chemical step. Second, elevated temperature likely enhances the swelling of the polymer matrix, which can alter internal diffusional pathways and resistance.

As a result of these combined effects, the intrinsic rate of the chemical reaction becomes comparable to the rate of mass transfer. This shift in the kinetic balance manifests as an increase in the apparent activation energy into the range of 20–40 kJ/mol, which is characteristic of a mixed diffusion-chemical control regime.

4.3. Comparative Analysis of Solvent and Solid-Phase Extraction Kinetics

A direct comparison reveals a fundamental trade-off between process intensity and operational simplicity.

Solvent extraction is characterized by fast kinetics (equilibrium within 2–3 min) and high efficiency (>90% for Lu), governed by a diffusion-controlled mechanism (E_a < 23.1 kJ/mol). This necessitates efficient agitation in mixer-settler units for industrial scale-up. Its main drawback is the reliance on volatile organic diluents (e.g., kerosene), which introduces environmental, safety, and health concerns, as well as complications in solvent management and recovery.

Solid-phase extraction, in contrast, offers diluent-free operation, reducing environmental footprint and simplifying waste handling. However, it exhibits slower kinetics (~60 min to equilibrium) and a more complex mechanism that transitions toward mixed chemical-diffusional control at higher temperatures (20–40 kJ/mol).

Consequently, solvent extraction is the preferred choice for high-throughput applications where maximizing processing speed and yield are paramount. Solid-phase extraction presents a viable and more sustainable alternative for niche applications, smaller-scale operations, or contexts with stringent environmental regulations, where its slower kinetics may be economically offset by the high value of the product or the operational benefits of eliminating organic solvents.

A comparative summary of the key kinetic and operational parameters for both methods is provided in Table 6.

Table 6. Comparative summary of solvent extraction and solid-phase extraction kinetics and key parameters for HREE recovery from phosphoric acid solutions.

Parameter/Characteristic	Solvent Extraction	Solid-Phase Extraction
Optimal temperature	298 K	298 K
Time to equilibrium	2–5 min	30–60 min
Kinetic regime	Diffusion-controlled (film diffusion)	Mixed (diffusion + chemical reaction)
Activation energy range	7.8–23.1 kJ/mol	2.3–40.7 kJ/mol *, temperature-dependent
Max. efficiency (e.g., Lu)	>90%	~40–50% (under tested conditions)
Key rate-limiting factor	Agitation intensity (mass transfer)	Combined pore diffusion and surface reaction
Primary practical advantage	Fast kinetics, high yield, established technology	No organic diluent, simpler waste handling, inherent safety

* Lower range corresponds to 298–318 K, higher range to 318–333 K.

5. Conclusions

This study provides such an analysis for heavy REEs from industrial phosphoric acid solutions derived from apatite processing using di-(2-ethylhexyl)phosphoric acid in both solvent and solid-phase extraction methods.

A distinct trend of progressively lower extraction efficiency with decreasing atomic number was observed, consistent with the diminishing chemical activity across the lanthanide series due to the lanthanide contraction.

For solvent extraction, the process kinetics exhibited a much stronger dependence on stirring intensity than on temperature. The low activation energies calculated (E_a < 23.1 kJ/mol) provide quantitative confirmation of a diffusion-controlled mechanism.

For solid-phase extraction, kinetic analysis via the Elovich and homogeneous particle diffusion models revealed a mechanism governed by a combination of film and intraparticle diffusion at lower temperatures, which shifts toward a mixed chemical-diffusional control at higher temperatures.

Based on the kinetic analysis, the following optimal conditions were established:

1. Solvent extraction: 298 K, 350 rpm, 20 vol.% D2EHPA in kerosene, V_{aq}:V_{org} = 2:1.
2. Solid-phase extraction: 298 K, 100 opm, solid-to-liquid ratio m:V = 1:10.

These results provide a scientific foundation for process design, directly informing critical engineering choices such as agitator specification, stage configuration, and temperature control to maximize recovery and selectivity.

To advance toward practical implementation, future work should focus on:

3. Designing a separation flowsheet using the established selectivity and optimal conditions for sequential HREEs recovery;
4. Assessing closed-cycle performance, including sorbent stability and stripping efficiency.

Author Contributions: O.C.: conceptualization, methodology, resources, supervision, project administration, funding acquisition; E.L.: software, formal analysis; investigation; writing—original draft preparation, visualization; V.S.: validation, data curation, formal analysis, writing—review and editing. All authors have read and agreed to the published version of the manuscript.

Funding: This research received no external funding.

Institutional Review Board Statement: Not applicable.

Informed Consent Statement: Not applicable.

Data Availability Statement: The original contributions presented in this study are included in the article. Further inquiries can be directed to the corresponding author.

Conflicts of Interest: The authors declare no conflicts of interest.

Abbreviations

The following abbreviations are used in this manuscript:

REEs	Rare earth elements
HREEs	Heavy rare earth elements
TREO	Total rare earth oxides
D2EHPA	Di-(2-ethylhexyl)phosphoric acid
rpm	Revolutions per minute
opm	Oscillations per minute

References

1. Liu, T.; Chen, J. Extraction and Separation of Heavy Rare Earth Elements: A Review. *Sep. Purif. Technol.* **2021**, *276*, 119263. [CrossRef]
2. Alves Dias, P.; Bobba, S.; Carrara, S.; Plazzotta, B. *The Role of Rare Earth Elements in Wind Energy and Electric Mobility*; Publication Office of the European Union: Luxembourg, 2020. [CrossRef]
3. Perrière, C.; Boulesteix, R.; Maître, A.; Jalocha, A. Study of Sintering Mechanisms of Ca-Doped Yttrium Aluminum Garnet Ceramics: From Nanostructure to Macroscopic Behaviour. *J. Eur. Ceram. Soc.* **2023**, *43*, 565–575. [CrossRef]
4. Savchenkov, S.A.; Bazhin, V.Y.; Povarov, V.G. Research on the Process of Gadolinium Recovery from the Melt of Salts on Formation of Mg–Zn–Gd Master Alloys for Manufacturing of Magnesium and Aluminium Special-Purpose Alloys. *Non-Ferr. Met.* **2020**, *1*, 35–40. [CrossRef]
5. Zhang, J.; Zhang, Z.; Xu, Y.; Wan, H.; Wang, J.; Zhang, L. Dissipative Soliton Resonance Ytterbium-Doped Fiber Laser with Cylindrical Vector Beam Generation. *Opt. Laser Technol.* **2019**, *113*, 234–238. [CrossRef]
6. Cherepovitsyn, A.; Solovyova, V. Prospects for the Development of the Russian Rare-Earth Metal Industry in View of the Global Energy Transition—A Review. *Energies* **2022**, *15*, 387. [CrossRef]
7. Lapinskas, A. Influence of Mining Rent on the Efficiency of Using Natural Potential: The Paradox of Plenty and Its Russian Specifics. *J. Min. Inst.* **2023**, *259*, 79–94. [CrossRef]
8. Reichl, C.; Schatz, M. (Eds.) *World Mining Data 2025*; Federal Ministry of Agriculture, Regions and Tourism: Vienna, Austria, 2025; 266p.
9. U.S. Geological Survey. *Mineral Commodity Summaries 2023*; U.S. Geological Survey: Reston, VA, USA, 2023; 210p. [CrossRef]
10. European Commission. *Study on the EU's List of Critical Raw Materials—Final Report*; Publications Office of the European Union: Luxembourg, 2020; 157p. [CrossRef]
11. McNulty, T.; Hazen, N.; Park, S. Processing the Ores of Rare-Earth Elements. *MRS Bull.* **2022**, *47*, 258–266. [CrossRef]
12. Xu, Z.; Li, G.; Yang, H.; Sha, A.; He, Z.; Tang, Y.; Wu, M.; Qu, J. Development Review on Leaching Technology and Leaching Agents of Weathered Crust Elution-Deposited Rare Earth Ores. *Minerals* **2023**, *13*, 1223. [CrossRef]
13. Lobacheva, O.L. Ion Flotation of Ytterbium Water-Salt Systems—An Innovative Aspect of the Modern Industry. *Water* **2021**, *13*, 3493. [CrossRef]
14. Dzhevaga, N.; Lobacheva, O. Reduction in Technogenic Burden on the Environment by Flotation Recovery of Rare Earth Elements from Diluted Industrial Solutions. *Appl. Sci.* **2021**, *11*, 7452. [CrossRef]
15. Chanturiya, V. Scientific Substantiation and Development of Innovative Processes for the Extraction of Zirconium and Rare Earth Elements in the Deep and Comprehensive Treatment of Eudialyte Concentrate. *J. Min. Inst.* **2022**, *256*, 505–516. [CrossRef]
16. Asadollahzadeh, M.; Shakib, B.; Torab-Mostaedi, M.; Outokesh, M. Extraction of Molybdenum (VI) and Vanadium (V) from Nitrate Solutions Using Coupling of Acid and Solvating Extractants. *Int. J. Eng.* **2019**, *32*, 1366–1371. [CrossRef]
17. Petrov, G.V.; Boduen, A.Y.; Fokina, S.B.; Zotova, I.E. Behaviour of Iridium and Ruthenium Complexes during Sorption in Sulphuric Acid Medium. *Non-Ferr. Met.* **2020**, *3*, 39–42. [CrossRef]
18. Lutskiy, D.S.; Ignatovich, A.S.; Sulimova, M.A. Determination of the Sorption Characteristics of Ammonium Perrenate Ions on Anion Exchange Resin AV-17-8. *J. Phys. Conf. Ser.* **2019**, *1399*, 055069. [CrossRef]
19. Babayan, I.I.; Kurdakova, S.V.; Kovalenko, N.A.; Uspenskaya, I.A. Bulk Properties of Di(2-Ethylhexyl)Phosphoric Acid–Samarium (Europium, Gadolinium) Di(2-Ethylhexyl)Phosphate–Organic Solvent Solutions. *Russ. J. Phys. Chem.* **2022**, *96*, 84–92. [CrossRef]
20. Fialkovsky, I.S.; Litvinova, T.E.; Lutsky, D.S.; Alexeev, A.A. Determination of the Parameters of Thermodynamic Stability Constants of Bromide Complexes of Rare Earth Metals for Modeling the Optimal Regimes of Hydrometallurgical Extraction. *Arab J. Basic Appl. Sci.* **2022**, *29*, 1–9. [CrossRef]
21. Mohammadzadeh, M.; Bagheri, H.; Ghader, S. Experimental Investigation and Thermodynamic Modeling of Zn^{+2} and Ni^{+2} Extraction from Zn Plant Residue Using D2EHPA. *Int. J. Eng.* **2023**, *36*, 2015–2027. [CrossRef]

22. Emsbo, P.; McLaughlin, P.I.; Bray, E.A.D.; Anderson, E.D.; Vandenbroucke, T.R.A.; Zielinski, R.A. Rare Earth Elements in Sedimentary Phosphorite Deposits A Global Assessment. In *Rare Earth and Critical Elements in Ore Deposits*; Society of Economic Geologists, Verplanck, P.L., Hitzman, M.W., Eds.; Reviews in Economic Geology; Society of Economic Geologists: Littleton, CO, USA, 2016; Volume 18, pp. 101–113.
23. Maksimova, V.; Krasavtseva, E.; Savchenko, Y.; Ikkonen, P.; Elizarova, I.; Masloboev, V.; Makarov, D. Study of the Composition and Properties of the Beneficiation Tailings of Currently Produced Loparite Ores. *J. Min. Inst.* **2022**, *256*, 642–650. [CrossRef]
24. Battsengel, A.; Batnasan, A.; Narankhuu, A.; Haga, K.; Watanabe, Y.; Shibayama, A. Recovery of Light and Heavy Rare Earth Elements from Apatite Ore Using Sulphuric Acid Leaching, Solvent Extraction and Precipitation. *Hydrometallurgy* **2018**, *179*, 100–109. [CrossRef]
25. Litvinova, T.E.; Gerasev, S.A. Behaviour of Cerium (III) Phosphate in a Carbonate-Alkaline Medium. *J. Min. Inst.* **2024**, *271*, 181–188.
26. Mukaba, J.-L.; Eze, C.P.; Pereao, O.; Petrik, L.F. Rare Earths' Recovery from Phosphogypsum: An Overview on Direct and Indirect Leaching Techniques. *Minerals* **2021**, *11*, 1051. [CrossRef]
27. Amirshahi, S.; Jorjani, E. Preliminary Flowsheet Development for Mixed Rare Earth Elements Production from Apatite Leaching Aqueous Solution Using Biosorption and Precipitation. *Minerals* **2023**, *13*, 909. [CrossRef]
28. Merroune, A.; Ait Brahim, J.; Achiou, B.; Boulif, R.; Mahdi Mounir, E.; Beniazza, R. Competitive Extraction and Stripping Behaviors of Rare Earth Elements from Industrial Wet-Process Phosphoric Acid Using Di-(2-Ethyl-Hexyl) Phosphoric Acid Solvent: Optimization and Thermodynamic Studies. *J. Mol. Liq.* **2022**, *367*, 120585. [CrossRef]
29. Yan, X.; Zhuang, H.; Wang, Y.; Wang, X.; Zhang, Z.; Yang, L. Kinetics and Mechanism on Removal of Aluminum from Phosphoric Medium by Solvent Extraction Using Lewis Cells. *Solvent Extr. Res. Dev. JPN* **2021**, *28*, 95–108. [CrossRef]
30. Yin, S.; Li, S.; Zhang, B.; Peng, J.; Zhang, L. Extraction Kinetics of Neodymium(III) from Chloride Medium in the Presence of Two Complexing Agents by D2EHPA Using a Constant Interfacial Area Cell with Laminar Flow. *Hydrometallurgy* **2016**, *161*, 160–165. [CrossRef]
31. Wu, F.; Liu, X.; Qu, G.; Ning, P. A Critical Review on Extraction of Valuable Metals from Solid Waste. *Sep. Purif. Technol.* **2022**, *301*, 122043. [CrossRef]
32. Sharifian, S.; Wang, N.-H.L. Resin-Based Approaches for Selective Extraction and Purification of Rare Earth Elements: A Comprehensive Review. *J. Environ. Chem. Eng.* **2024**, *12*, 112402. [CrossRef]
33. Miyagawa, A.; Kusano, Y.; Nakagawa, R.; Nagatomo, S.; Sano, Y.; Nakatani, K. Kinetically Revealed Transfer Mechanism of Europium(III) in Tributyl Phosphate Microdroplet/NaNO3 Aqueous Solution System by Fluorescence Microspectroscopy. *J. Mol. Liq.* **2022**, *352*, 118757. [CrossRef]
34. Xiao, C.; Huang, K.; Liu, H. A Novel Constant Interfacial Area Cell for Determining the Extraction Kinetics of Er(III) from Chloride Medium. *Chin. J. Chem. Eng.* **2018**, *26*, 1435–1441. [CrossRef]
35. Yin, S.; Li, S.; Zhang, B.; Peng, J.; Zhang, L. Mass Transfer Kinetics of Lanthanum (III) Extraction in the Presence of Two Complexing Agents by D2EHPA Using a Constant Interfacial Area Cell with Laminar Flow. *Chem. Eng. Res. Des.* **2015**, *104*, 92–97. [CrossRef]
36. Kao, H.-C.; Yen, P.-S.; Juang, R.-S. Solvent Extraction of La(III) and Nd(III) from Nitrate Solutions with 2-Ethylhexylphosphonic Acid Mono-2-Ethylhexyl Ester. *Chem. Eng. J.* **2006**, *119*, 167–174. [CrossRef]
37. Cheremisina, O.; Sergeev, V.; Ponomareva, M.; Ilina, A.; Fedorov, A. Kinetics Study of Solvent and Solid-Phase Extraction of Rare Earth Metals with Di-2-Ethylhexylphosphoric Acid. *Metals* **2020**, *10*, 687. [CrossRef]
38. Satpathy, S.; Mishra, S. Kinetics and Mechanisms of Solvent Extraction and Separation of La(III) and Ni(II) with DEHPA in Petrofin. *Trans. Nonferrous Met. Soc. China* **2019**, *29*, 1538–1548. [CrossRef]
39. Asadollahzadeh, M.; Torkaman, R.; Torab-Mostaedi, M. Optimization of Green Technique Develop for Europium (III) Extraction by Using Phosphonium Ionic Liquid and Central Composite Design Approach. *Int. J. Eng.* **2021**, *34*, 508–516. [CrossRef]
40. Zelikman, A.N.; Voldman, G.M.; Belyaevskaya, L.V. *Theory of Hydrometallurgical Processes*; Metallurgiya: Moscow, Russia, 1983; 424p, ISBN 978-5-7996-3553-4.
41. Wieszczycka, K.; Filipowiak, K.; Aksamitowski, P.; Wojciechowska, I. Task-Specific Ionic Liquid Impregnated Resin for Zinc(II) Recovery from Chloride Solutions. *J. Mol. Liq.* **2020**, *299*, 112115. [CrossRef]
42. Masoud, A.M.; Ammar, H.; Elzoghby, A.A.; El Agamy, H.H.; Taha, M.H. Rare Earth Elements Adsorption from Phosphoric Acid Solution Using Dendrimer Modified Silica Gel as Well as Kinetic, Isotherm, and Thermodynamic Studies. *J. Rare Earths* **2024**, *43*, S1002072124001832. [CrossRef]
43. Juang, R.-S.; Chen, M.-L. Application of the Elovich Equation to the Kinetics of Metal Sorption with Solvent-Impregnated Resins. *Ind. Eng. Chem. Res.* **1997**, *36*, 813–820. [CrossRef]
44. Wu, F.-C.; Tseng, R.-L.; Juang, R.-S. Initial Behavior of Intraparticle Diffusion Model Used in the Description of Adsorption Kinetics. *Chem. Eng. J.* **2009**, *153*, 1–8. [CrossRef]

45. Gonzalez-Luque, S.; Streat, M. Uranium Sorption from Phosphoric Acid Solutions Using Selective Ion Exchange Resins. *Hydrometallurgy* **1983**, *11*, 207–225. [CrossRef]
46. Cortina, J.L.; Arad-Yellin, R.; Miralles, N.; Sastre, A.M.; Warshawsky, A. Kinetics Studies on Heavy Metal Ions Extraction by Amberlite XAD2 Impregnated Resins Containing a Bifunctional Organophosphorous Extractant. *React. Funct. Polym.* **1998**, *38*, 269–278. [CrossRef]
47. Benamor, M.; Bouariche, Z.; Belaid, T.; Draa, M.T. Kinetic Studies on Cadmium Ions by Amberlite XAD7 Impregnated Resins Containing Di(2-Ethylhexyl) Phosphoric Acid as Extractant. *Sep. Purif. Technol.* **2008**, *59*, 74–84. [CrossRef]
48. Zhou, J.; Zhang, X.; Deng, B.; Huang, Y.; Liu, X.; Ning, S.; Kuang, S.; Liao, W. Separation and Purification of Heavy Rare Earth Elements by a Silica/Polymer-Based β-Aminophosphonic Acid Resin from Chloride Media. *Sep. Purif. Technol.* **2025**, *354*, 129342. [CrossRef]
49. Tseng, R.-L.; Tran, H.N.; Juang, R.-S. Revisiting Temperature Effect on the Kinetics of Liquid–Phase Adsorption by the Elovich Equation: A Simple Tool for Checking Data Reliability. *J. Taiwan Inst. Chem. Engrs.* **2022**, *136*, 104403. [CrossRef]
50. Maslova, M.V.; Ivanenko, V.I.; Gerasimova, L.G. Effect of Temperature on the Kinetics of Strontium Cation Sorption by a Titanium Phosphate-Based Sorbent. *Russ. J. Phys. Chem. A* **2019**, *93*, 1002–1008. [CrossRef]

Disclaimer/Publisher's Note: The statements, opinions and data contained in all publications are solely those of the individual author(s) and contributor(s) and not of MDPI and/or the editor(s). MDPI and/or the editor(s) disclaim responsibility for any injury to people or property resulting from any ideas, methods, instructions or products referred to in the content.